INT. J. GEOGRAPHICAL INFORMATION SCIENCE, 2003
VOL. 17, NO. 1, 1–23

Taylor & Francis
Taylor & Francis Group

Research Article

Vectorial algebra algorithms for calculating terrain parameters from DEMs and solar radiation modelling in mountainous terrain

JAVIER G. CORRIPIO
Centre d'Etudes de la Neige, Météo France/CNRM, 1441 rue de la piscine, 38406 St Martin d'Heres, CEDEX, France

(*Received 24 July 2001; accepted 13 May 2002*)

Abstract. Terrain parameters derived from digital elevation models (DEMs), such as slope gradient, aspect and cell surface area, are represented as a vector normal to the surface and calculated using the minimum areal unit of the DEM, that is enclosed between four data points. The position of the Sun is calculated by applying rotational matrices to a unit vector defined at noon as a function of latitude and declination. The direct component of insolation intercepted by the cell surface is then calculated as a dot product between the unit vector in the direction of the Sun and the unit vector normal to surface, multiplied by direct normal irradiation. Hillshading is computed by scanning the projection of cells onto a solar illumination plane perpendicular to the Sun direction. Horizon angles and estimated sky view factor are calculated using a more economical algorithm than a rigorous evaluation of all the angles subtended by every grid cell to each other. The performance of the slope algorithm is evaluated using a synthetic surface and real world examples are given for the Mont Blanc Massif, in the French Alps.

1. Introduction

Digital elevation models (DEMs) are mathematical models of the Earth's surface that, at present, are the most powerful method of representing relief (Stocks and Heywood 1994). They are extensively used in environmental modelling and play an important role in geographic information systems (GIS).

Terrain parameters such as slope gradient and orientation of slope (aspect) are important controls in a number of surface processes, such as water runoff, erosion (Moore *et al.* 1993) and incoming solar radiation (Nuñez 1980, Barry 1992). These factors alone or combined are major controls in biological, glaciological and geomorphological processes, and thus have a decisive influence in biodiversity (Kumar and Skidmore 2000), tree line height (Kirckpatrick and Nuñez 1980), human settlement, fauna distribution (Stefanovič and Wiersema 1985), tourism and recreation (e.g. ski slopes), local climatic conditions (Barry 1992), snow line and glacier mass balance (Willis *et al.* 1998, Brock *et al.* 2000).

It is therefore understandable that considerable effort has been expended in developing fast and efficient algorithms to calculate the gradient of the surface from DEMs (Skidmore 1989) and the variation of surface solar radiation with topography

International Journal of Geographical Information Science
ISSN 1365-8816 print/ISSN 1362-3087 online © 2003 Taylor & Francis Ltd
http://www.tandf.co.uk/journals
DOI: 10.1080/13658810210157796

(Williams *et al.* 1972, Nuñez 1980, Dozier and Frew 1990, Duguay 1995, Varley *et al.* 1996, Kumar *et al.* 1997).

Mountainous terrain is characterized by irregular and rapid changes in elevation over short distances. It is an environment where thresholds play an important role, for example in the influence of slope on landslides or avalanches (Wadge 1988, Dakhal *et al.* 2000). It is desirable to derive terrain parameters for these regions using algorithms that retain real extreme values minimizing any smoothing effect. Many methods for calculating slope from DEMs are based on a 3×3 kernel or 'roving window' displaced along the grid cells (Evans 1980, Horn 1981, Zevenbergen and Thorne 1987, Skidmore 1989). This approach has the advantage of minimising the effect of data errors in general, as it takes into consideration the 8 surrounding points to a given one (Horn 1981). However, as Hodgson (1995) has shown, the undesirable side effect is the computation of the slope for an equivalent area of up to twice the cell size. These methods also tend to underestimate slope on rough terrain and in coarse resolution grids (Chang and Tsai 1991, Gao 1997). According to Hodgson's (1995) work, the most accurate algorithms for the combined estimation of surface and slope are those which use the four nearest neighbour elevations in the grid. On most applications a compromise will be required between the original data quality and the accuracy or degree of smoothing of slope calculation algorithms. By using just one cell, the user keeps the final decision, as to whether the results are reliable or it is advisable to perform any further filtering or smoothing.

This paper presents an algorithm for calculating the gradient of the surface using the minimum areal unit in a DEM, that of the surface enclosed between four data points. To avoid confusion by the different definitions of the word gradient (Burrough 1986, p. 50), when used alone in this paper it refers to the mathematical definition, and in this particular case, the gradient is defined as a three dimensional unit vector perpendicular to the surface. From this vector slope and aspect can be calculated, although this step is unnecessary for solar radiation modelling using the Sun position algorithm derived here. The Sun position is defined as another unit vector in its direction, and thus, finding the angle between the Sun and the normal to surface is equivalent to finding the solution to a dot product between both vectors. These algorithms make optimal use of the array handling power of modern computer programming languages, allowing fast implementation and running times. Furthermore the concept is easy to grasp and visualize.

2. Vector defining an inclined surface

We consider the smallest surface unit in a regularly gridded DEM as the plane enclosed by four data points: $z_{i,j}$, $z_{i+1,j}$, $z_{i,j+1}$, $z_{i+1,j+1}$, where $z_{i,j}$ is the elevation of a point at row i, column j (see figure 1). Although it would be possible to extend the surface division into a triangular mesh (Wang *et al.* 2000a), we prefer to keep the cell as the surface area unit for compatibility with other applications, such as raster information extracted from orthorectified photographs or satellite images, and for compatibility with existing models in glaciology, hydrology or snow studies, which are cell based (Arnold *et al.* 1996, Richards *et al.* 1996, Purves *et al.* 1998). It is also unreliable interpolating values from the interior of a cell in mountain areas, characterized by non-uniform change. However, as a plane is defined by three points in space, then the four points at the corners of the grid cell may delimit more than one single plane. As the resolution of the data does not permit defining the geometry of the area enclosed, a good approximation is to find an average between the two triangles

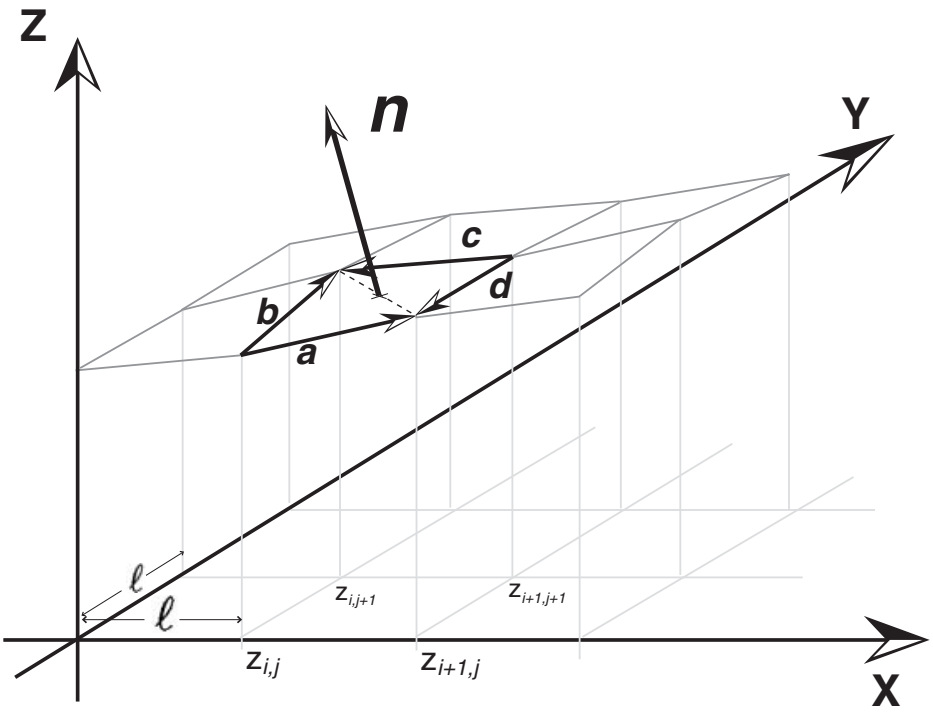

Figure 1. Vector normal to a grid cell surface. Vector **n** is the average of cross products $\mathbf{a}\times\mathbf{b}$ and $\mathbf{c}\times\mathbf{d}$. Its length approximates the surface area of the grid cell with accuracy depending on resolution.

at both sides of the cell diagonal. It can be shown that the result is the same whichever diagonal we choose. A vector normal to these surfaces is defined by half the sum of cross products of vectors along the sides of the grid cell, defined as in equation (1). In figure 1 these triangular surfaces are comprised between vectors **ab** and **cd**. The gradient will be the average of cross products $\mathbf{a}\times\mathbf{b}$ and $\mathbf{c}\times\mathbf{d}$. Ritter (1987) has previously used a vector based approach, although the approach taken in this paper differs in the selection of points to compute the slope and in the subdivision of the cell into two planes. The computation of surface area is also a new addition.

The resulting vector of a cross product has the length of the parallelogram whose sides are the vector factors. Thus, the modulus of the vector normal to surface calculated in this way will approximate the value of the surface area of the grid cell with accuracy proportional to the resolution of the grid.

In a regular square grid of cell size l, as in figure 1, the x, y, z components of the vectors along the side of the grid cell are defined as:

$$\begin{cases} \mathbf{a}=(l,\,0,\,\Delta z_a), & \text{with } \Delta z_a = z_{i+1,\,j} - z_{i,\,j} \\ \mathbf{b}=(0,\,l,\,\Delta z_b), & \text{with } \Delta z_b = z_{i,\,j+1} - z_{i,\,j+1} \\ \mathbf{c}=(-l,\,0,\,\Delta z_c), & \text{with } \Delta z_c = z_{i,\,j+1} + z_{i+1,\,j+1} \\ \mathbf{d}=(0,\,-l,\,\Delta z_d), & \text{with } \Delta z_d = z_{i+1,\,j} - z_{i+1,\,j+1} \end{cases} \tag{1}$$

The vector normal to the grid cell, **n**, will be:

$$\mathbf{n}=\frac{(\mathbf{a}\times\mathbf{b})}{2}+\frac{(\mathbf{c}\times\mathbf{d})}{2}=\frac{1}{2}\begin{vmatrix}\mathbf{i} & \mathbf{j} & \mathbf{k}\\ l & 0 & \Delta z_a\\ 0 & l & \Delta z_b\end{vmatrix}+\frac{1}{2}\begin{vmatrix}\mathbf{i} & \mathbf{j} & \mathbf{k}\\ -l & 0 & \Delta z_c\\ 0 & -l & \Delta z_d\end{vmatrix} \tag{2}$$

Simplifying the result of equation (2) gives the components of the vector normal to surface in terms of grid elevation points and cell spacing as:

$$\mathbf{n}=\begin{pmatrix}1/2\,l(z_{i,j}-z_{i+1,\mathrm{j}}+z_{i,j+1}-z_{i+1,j+1})\\ 1/2\,l(z_{i,j}+z_{i+1,j}-z_{i,j+1}-z_{i+1,j+1})\\ l^2\end{pmatrix} \tag{3}$$

The surface area of this cell will be $|\mathbf{n}|$, the length of vector **n**. The unit vector in the direction of **n** will be denoted $\mathbf{n}_u$.

This algorithm makes optimal use of the array handling capabilities of many computer languages and can be implemented very efficiently. The CPU time used for processing a DEM of about 250 000 cells, implementing the algorithm in IDL, on a Sun Enterprise 450 workstation was about 0.5 seconds excluding data input, and another half a second for the computation of the corresponding unit vectors and the area of every cell. Figure 2 shows a grey-scale representation of every component of the vector gradient for a DEM of the Mont Blanc Massif, French Alps, while figure 3 shows the derived aspects.

If the slope and aspect of the surface need to be used, these can be calculated from the components of $\mathbf{n}_u$ as follows:

$$\varsigma=\cos^{-1}n_{uz}, \tag{4}$$

where ς is the slope and n_{uz} is the z coordinate of vector $\mathbf{n}_u$.

The aspect ϕ is not defined for slopes of 0°, a vertical vector gradient. In any other case it can be calculated from the x, y components of $\mathbf{n}_u$. To make the gradient vector compatible with the Sun vector, a left handed coordinate system has been chosen, with the X-axis (columns) increasing eastwards and the Y-axis (rows) increasing southwards. Counting clockwise from north, the aspect would be:

$$\phi=\frac{\pi}{2}+\tan^{-1}\frac{n_{uy}}{n_{ux}}. \tag{5}$$

The sign of the coordinates needs to be taken into account to decide in which quadrant the vector lies. The tangent is not defined when the horizontal projection of $\mathbf{n}_u$ lies on the Y-axis ($n_{ux}=0$) and it is ambiguous when it lies on the X-axis. Alternatively, a ratio between the sine and cosine of $\mathbf{n}_{uxy}$ could be used (Horn 1981). The above coordinate system is a mirror image of those commonly used in DEMs, with the Y-axis increasing northwards. To apply equation (5) in this case we only need to invert the y-coordinate of vector $\mathbf{n}_u$. The graphic visualisation of these results are shown in figures 2(*c*) and 3.

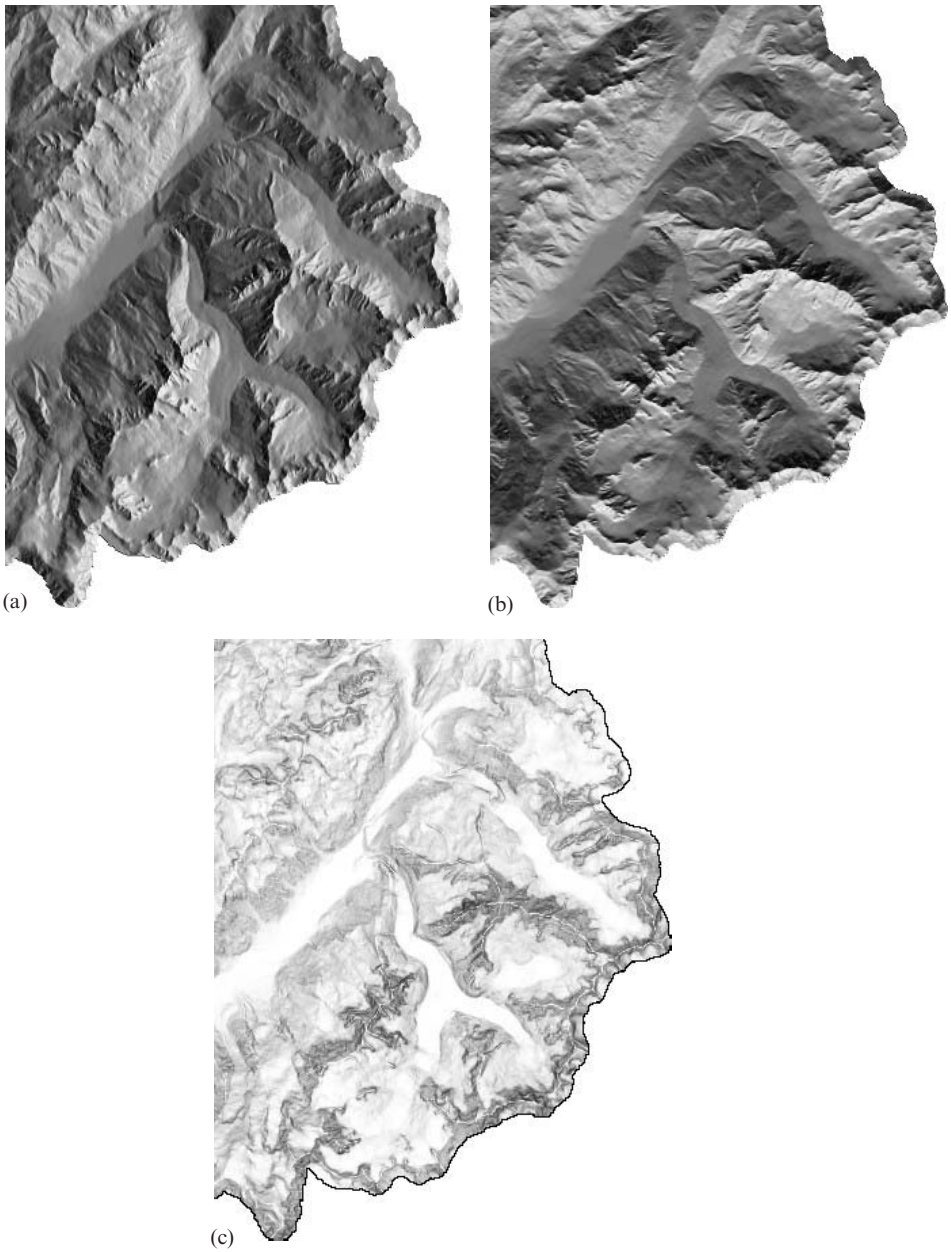

Figure 2. Relative grey-scale representation of the values of coordinates x, y, z for the vector normal to surface in a digital elevation model of the Mont Blanc Massif. To make the coordinates agree with solar position convention, white is a high positive eastwards, southwards and upward component. The grid is 338 columns by 444 rows, with a resolution of 50 m (16.9×22.2 km). The inverted Y-shaped feature in the lower centre is the Mer de Glace, the largest glacier in the French Alps. The sharp border on the right and lower areas is the national boundary plus a buffer area, as the relief of Italy and Switzerland is not shown, and the main valley running NE to SW is the Valley of Chamonix. North is up.

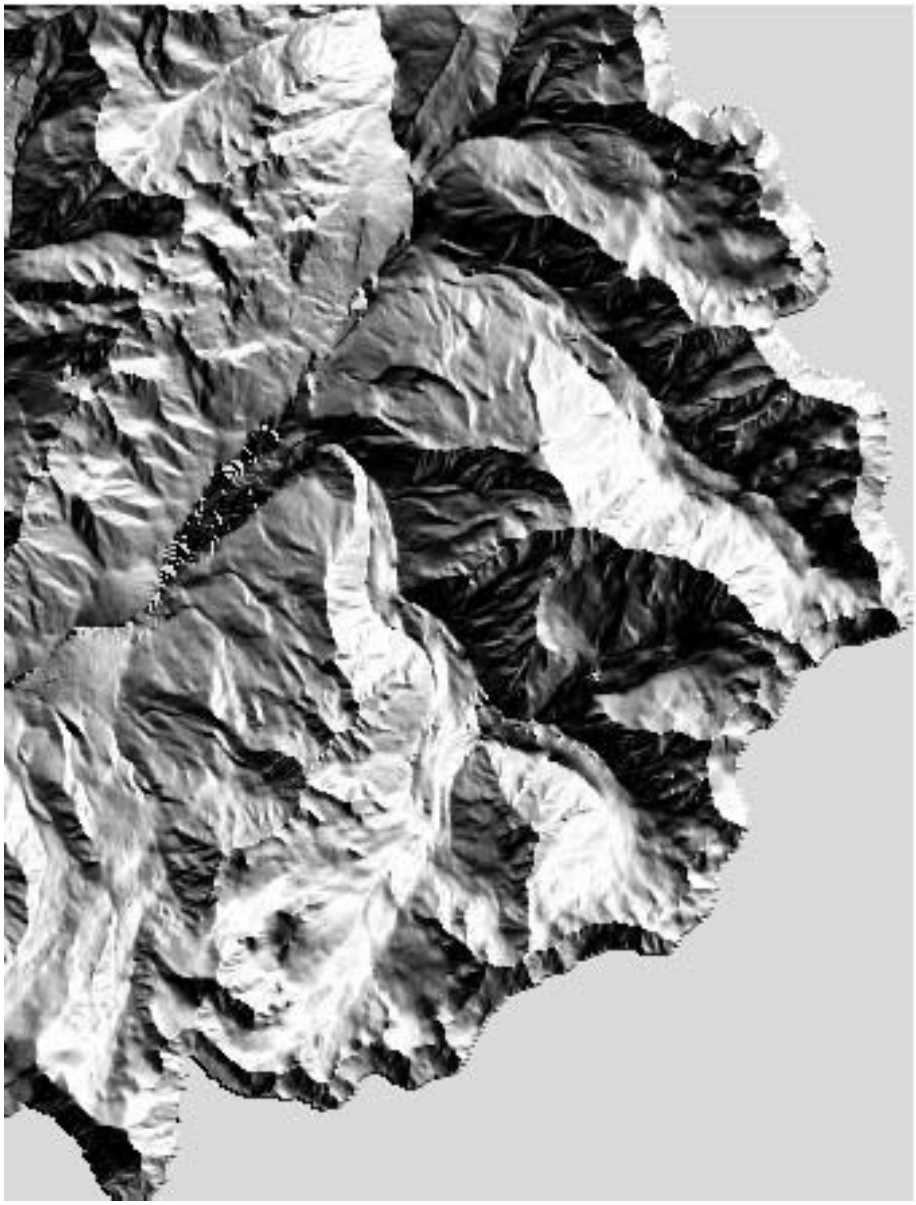

Figure 3. Relative grey-scale representation of surface aspects in the Mont Blanc DEM. White is North-east and black is South-west.

3. Vector defining the position of the Sun

The vector in the direction of the Sun can be calculated from the solar azimuth and zenith angles (Horn 1981, Paterson *et al.* 1985, Wang *et al.* 2000b), and these angles can be calculated using spherical trigonometry (Nautical Almanac Office 1974, Iqbal 1983). However, for completeness and consistency with the vectorial approach, a new procedure is explained here. We define a topocentric coordinate system as an orthogonal reference system with origin at the observer position on

the surface of the Earth (figure 4). To follow the conventions normally used in solar radiation studies regarding the position of the Sun (Iqbal 1983, p. 15), the coordinate axes are defined as follows:

- the X-axis is tangential to the Earth's surface in direction East–West and positive eastwards;
- the Y-axis is tangential in direction North–South and positive southwards;
- and the Z-axis lies along the Earth's radius and is positive upwards.

By definition, the Sun lies on the ZY-plane (i.e. it is on the vertical plane) at noon local apparent time (LAT). At this time, the x-coordinate of a unit vector pointing to the Sun (solar vector from now on) will be null. The solar declination (δ) is the angle between the solar rays and the plane of the Earth's equator. The

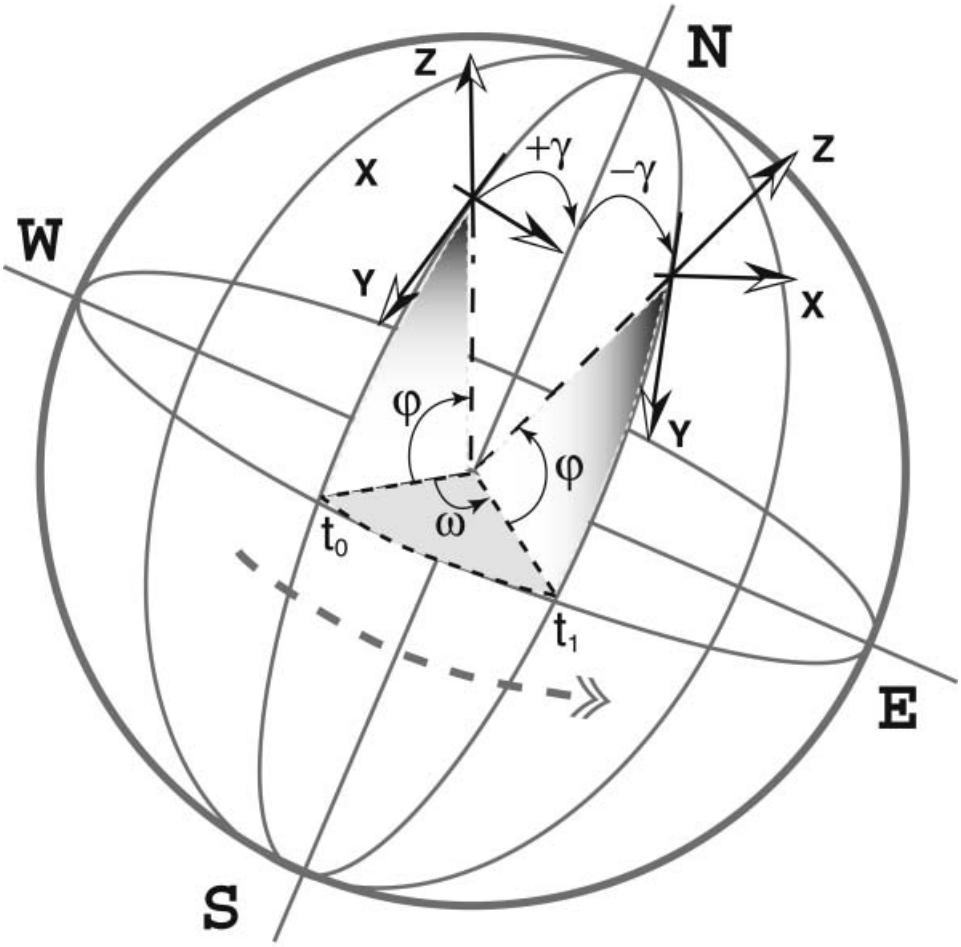

Figure 4. Rotation of the topocentric coordinate system XYZ at angle ω, from time t_0 to time t_1. This movement can be decomposed in three rotations: (*i*) rotation around axis X at angle $\gamma = \pi/2 - \varphi$, where φ is the latitude; (*ii*) rotation around axis Z at angle ω; and (*iii*) rotation back around axis X at angle $-\gamma$. Translation is ignored as the maximum parallax of the Earth is 8.8 seconds of arc (Nautical Almanac Office 1974), and therefore negligible for most solar radiation applications.

geographical latitude (φ) is the angle between the radius of the Earth at the observer position (that is the Z-axis in our coordinate system) and the equatorial plane. Thus, the solar vector, $\mathbf{s}_0$, at noon LAT will be:

$$\mathbf{s}_0 = (0, \sin(\varphi - \delta), \cos(\varphi - \delta)). \tag{6}$$

At any given time t, the Earth will have rotated away from noon at hour angle ω at an angular speed of 2π radians or 360° per day. The hour angle is the angle between the observer meridian and the solar meridian, the convention is that ω is zero at noon and positive before noon (Iqbal 1983, p. 15). At this time the topocentric coordinate system will have changed position in relationship to the Sun at noon. This movement can be decomposed in three rotations (see figure 4): one around the X-axis, to place the Z-axis parallel to the axis of rotation of the Earth; a second rotation around the Z-axis at angle ω and a third rotation back around the X-axis to the observer position. To find the coordinates of the solar vector in the new, rotated reference system we multiply the original coordinates by three rotational matrices describing these movements. For a brief description of rotational matrices, a common procedure in computer graphics, see for example Foley *et al.* (1990) and related references. Thus, at any time, and assuming no atmospheric refraction, the solar vector $\mathbf{s}$ will be:

$$\mathbf{s} = r_x(\gamma) r_z(\omega) r_x(-\gamma) \mathbf{s}_0, \tag{7}$$

where r is a rotation matrix around axis in subscript and angle in brackets, γ is the angle between Earth's axis and the topocentric coordinate system Z-axis, and the hour angle ω is zero at noon and has the following value in radians at any time t (LAT) given in hours and decimal fraction:

$$\omega = \pi \left(\frac{t}{12} - 1 \right) \tag{8}$$

In matrix notation:

$$\mathbf{s} = \begin{pmatrix} 1 & 0 & 0 \\ 0 & \cos\gamma & -\sin\gamma \\ 0 & \sin\gamma & \cos\gamma \end{pmatrix} \begin{pmatrix} \cos\omega & -\sin\omega & 0 \\ \sin\omega & \cos\omega & 0 \\ 0 & 0 & 1 \end{pmatrix} \begin{pmatrix} 1 & 0 & 0 \\ 0 & \cos(-\gamma) & -\sin(-\gamma) \\ 0 & \sin(-\gamma) & \cos(-\gamma) \end{pmatrix} \begin{pmatrix} s_{0x} \\ s_{0y} \\ s_{0z} \end{pmatrix} \tag{9}$$

This rotation of the Earth also involves a translation of the defined reference system, $\mathbf{s}_0$, but the maximum parallax of the Earth is $8.8''$ of arc (Nautical Almanac Office 1974), that is $4.4''$ if we take as reference noon for the hour angle. This is much smaller than the precision of other quantities involved, so the extra computational effort to account for this translation can be saved for most applications.

This equation can be fed directly into most programming languages, simplifying the programming effort, or can be solved for every coordinate (see Appendix A). In this case, the values for the x, y, z coordinates of the solar vector would be:

$$\mathbf{s} = \begin{pmatrix} -\sin\omega\cos\delta \\ \sin\varphi\cos\omega\cos\delta - \cos\varphi\sin\delta \\ \cos\varphi\cos\omega\cos\delta + \sin\varphi\sin\delta \end{pmatrix} \tag{10}$$

From this equation, the solar zenith angle θ can be calculated as:

$$\theta = \cos^{-1} s_z, \tag{11}$$

and the solar azimuth ϕ as:

$$\phi = \frac{\pi}{2} + \tan^{-1} \frac{s_y}{s_x} \tag{12}$$

where s_x, s_y and s_z are the coordinates of the solar vector.

Due to the obliquity of the ecliptic, the declination can change from $-23^\circ 26' 12''$ at the winter solstice (Northern Hemisphere) to $+23^\circ 26' 12''$ at the summer solstice, with a variation of less than $10''$ over the next 20 years due to precession and nutation in the obliquity of the ecliptic and to general precession of the longitude of the Sun (Nautical Almanac Office 1974). Calculating the declination is not a trivial problem, as its value is affected by long-term orbital changes (i.e. at Milankovitch time scales) and by the interaction with the Moon and other planets.

Many authors have given different solutions to the problem of finding the solar declination with different degrees of accuracy (Spencer 1971, Walraven 1977, Page 1986). Here a Fourier series approximation derived by Bourges (1985) that estimates the declination with a mean error of 0.008° and a maximum error of 0.02° is used. Bourges explains clearly the procedure and astronomical assumptions, so that the series can be corrected for the required epoch. For the present day, we have:

$$\begin{aligned} \delta = {} & 0.3723 \\ & + 23.2567 \sin D - 0.758 \cos D \\ & + 0.1149 \sin 2D + 0.3656 \cos 2D \\ & - 0.1712 \sin 3D + 0.0201 \cos 3D, \end{aligned} \tag{13}$$

where D is the day number:

$$D = (360/365.25) \times (J - 79.346), \tag{14}$$

and J is the Julian day, 1 on the first of January and 365 on the 31st of December (more strictly, the difference between the Julian day in consideration and the Julian day on January the first at noon for that given year, plus 1).

The maximum daily variation in declination is less than 0.5° of arc at the equinoxes and less than 1 minute of arc at the solstices (Spencer 1971), thus, when accuracy to the nearest degree is required, a single value of δ can be used over a whole day, with considerable simplification in the calculations. To keep within an error similar to that of the selected method of calculating declination, the coordinates of the Sun vector at noon ($\mathbf{s}_0$) can be recalculated every time, adding to the day number $t/24$ days, where t is the number of hours from noon LAT.

In order to integrate the amount of solar radiation over the whole day, it is necessary to know the duration of daylight and therefore the time of sunrise and

sunset. Astronomical sunrise and sunset will occur at the time when the z coordinate of the Sun vector equals zero. Thus, solving for z in equation (10):

$$z = \cos\varphi \cos\omega \cos\delta + \sin\varphi \sin\delta = 0, \tag{15}$$

gives:

$$\cos\omega = \frac{-\sin\varphi \sin\delta}{\cos\varphi \cos\delta}, \tag{16}$$

$$\omega = \cos^{-1}(-\tan\varphi \tan\delta), \tag{17}$$

which is the absolute value of the hour angle at sunrise or sunset. Note that this solution is in agreement with the results derived following spherical trigonometrical equations (e.g. Iqbal 1983, p. 16).

The sunrise will be at $t = 12(1-\omega/\pi)$ hours and the sunset at $t = 12(1+\omega/\pi)$. The day length will be $2\omega 2\pi/24$. The equation has no solution if $|-\tan\varphi \tan\delta| > 1$, in this case, if the latitude has the same sign of the declination, that is, $\varphi/|\varphi| = \delta/|\delta|$ it is the polar day, and if they are of different sign then it is the polar night. These equations do not take into account the height of the observer above the horizon or crepuscular diffuse solar irradiation: for a detailed treatment of the astronomical parameters involved in this case, see the Nautical Almanac Office (1974).

3.1. *Angle of incidence of the Sun on inclined surfaces*

The fraction of light intercepted by the inclined surface will be proportional to the cosine of the angle between the normal to the surface and the sun rays. Having calculated a unit vector gradient normal to the surface and a unit vector in the direction of the Sun, the dot product of both gives the cosine of the angle between them; thus the angle between the Sun and the normal to surface, θ_s is:

$$\theta_s = \cos^{-1}(\mathbf{s} \cdot \mathbf{n}_u) \tag{18}$$

Figure 5 shows the application of these algorithms to produce a map of solar radiation over an area of high relief, the Mont Blanc Massif in the French Alps. Incoming solar radiation was modelled for clear skies at 15-minute intervals from sunrise to sunset at the time of the spring equinox, following an updated parametric model based on Iqbal (1983). Irradiation at every grid cell is evaluated according to the angle of incidence of the Sun and the shading of surrounding terrain as described in §4. Diffuse incoming solar radiation is evaluated according to the hemispherical portion of sky visible from every grid cell as described in §5.

4. Shaded relief

The Sun can be considered as a point light source at infinite distance, and thus, all illumination rays arriving at a grid can be considered parallel. For computational convenience we consider an 'illumination plane' perpendicular to the solar rays (figure 6). All solar rays traverse this plane at a right angle. By checking the projection of a grid cell over this plane, following the direction of the Sun, we can determine whether a point is in the Sun or in the shade of another cell. In figure 6 this is illustrated for a two-dimensional example: the projection of P_1, that is, P'_1, has a value higher than any previous one (as it is the first point to be scanned), so it is in the Sun. Similarly for P'_2 and P'_3, however, P'_4 has a lower value than P'_3 and therefore is in its shadow. The projection of a point P'_i on the solar plane **SP** is the dot product of the vector $\mathbf{OP}_i$ and the unit vector $\mathbf{s}_p$, which is a vector in the direction of the

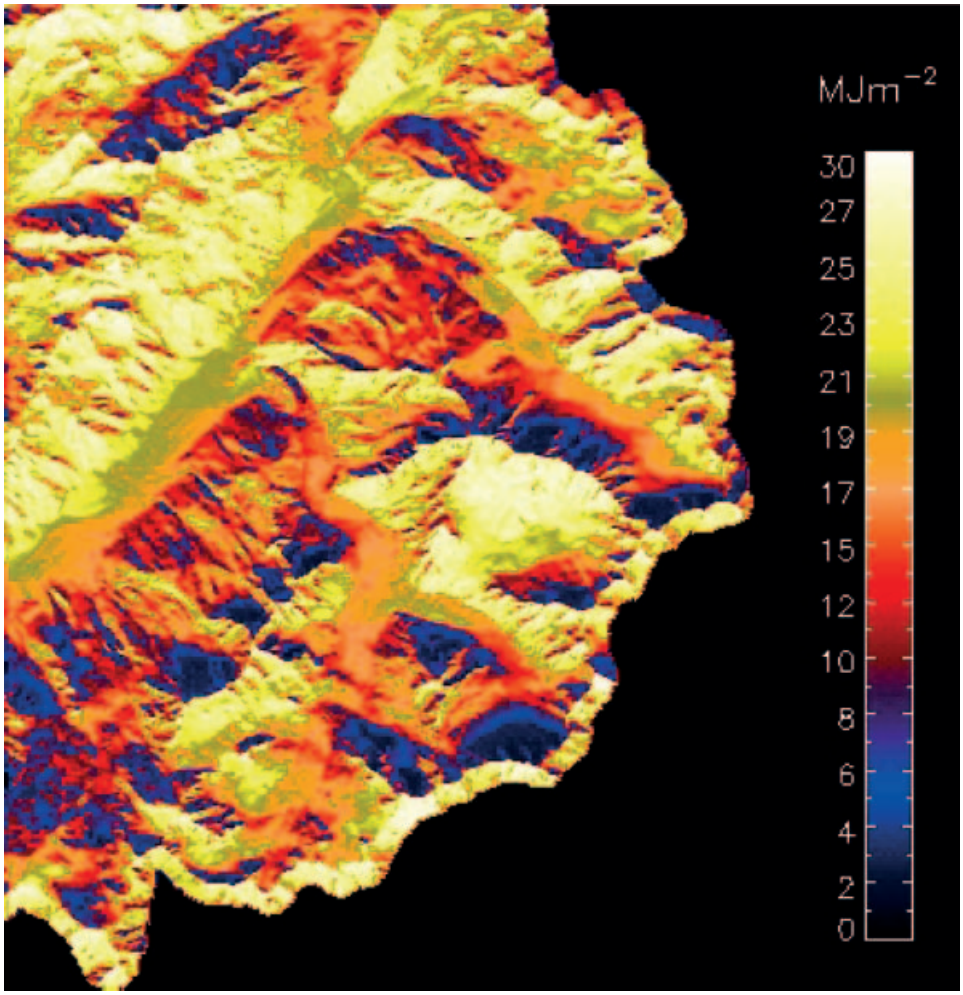

Figure 5. Colour coded map of insolation received at the Mont Blanc Massif at the spring equinox. Incoming solar radiation is modelled for clear skies at 15 minutes interval from sunrise to sunset following Iqbal's (1983) parametric model. Incident solar radiation for every grid cell is evaluated according to the angle of incidence of the Sun and the shading of surrounding terrain. Diffuse incoming solar radiation is evaluated according to the hemispherical portion of sky visible from every grid cell. Reflected radiation from surrounded terrain is not computed. Values range from 2.2 to 29.96 M Jm^{-2}.

plane **SP** and perpendicular to the solar vector **s**. A cell will shade itself if the angle between the Sun and the vector normal to the cell's surface is higher than $\pi/2$.

By scanning the grid across the Sun path, we can determine which cells are shaded or not by comparing their projection values. In order to speed up the implementation of the algorithm, an array of cells is defined for every cell on the Sun side of the grid border. The length of this array is given by the first intersection of a line along the vector opposite to the Sun and the DEM boundaries. The x, y position of the cells under consideration in the original grid are estimated by integer increments of the vector opposite to the Sun for the largest x, y coordinate. Figure 7

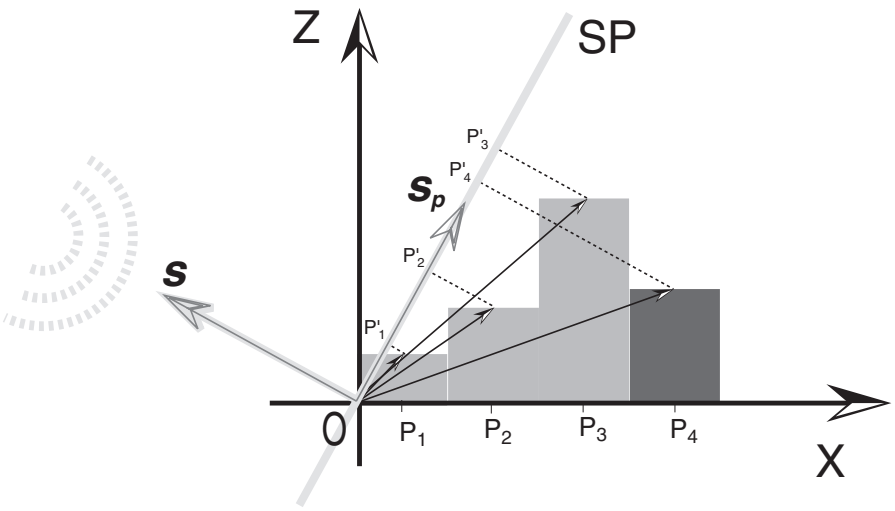

Figure 6. Hillshading. As the Sun can be considered as a point source at infinite distance, all solar rays are parallel and cross the plane **SP** perpendicularly. By checking the projection of a grid cell over this plane we can determine whether a point is in the Sun or in the shade of a previous cell. In the figure the projection of P_1, that is P'_1, has a value higher than any previous one (as it is the first point to be scanned), so it is in the Sun. Similarly for P'_2 and P'_3, however, P'_4 has a lower value than P'_3 and therefore is in its shadow. The projection of a point P'_i on the 'solar plane' **SP** is the dot product of the vector $\mathbf{OP}_i$ and the vector $\mathbf{s}_p$, which is a unit vector perpendicular to $\mathbf{s}$, the unit vector in the direction of the Sun.

shows the application of the hillshading algorithm to the Mont Blanc Massif DEM. The Sun is assumed to be at 315° (north-west) and the zenith angle is 45°, an unrealistic position traditionally chosen to avoid a pseudoscopic effect, that is the reversal of the relief or valleys appearing like mountains and mountains looking like valleys when illumination is applied from the south. The image has a minimum illuminance of 18% to account for diffuse radiation and the reflected light is modified according to $\cos\theta_s$. Computation time was about one-sixth of a second for a grid of 150 000 cells (figure 7) on an Intel Xeon CPU 2 GHz 523 276 KB RAM and 1.6 seconds on a SunSparc 450.

The coordinates of the vectors involved in these calculations for the three dimensional case are as follows: the vector from the origin to any point $P_{i,j}$ at column i, row j is:

$$\mathbf{P}_{i,j} = (l_i, l_j, z_{i,j}), \tag{19}$$

where l is the cell size and $z_{i,j}$ the elevation of cell at i, j. For simplicity we assume that the solar plane crosses the grid at the origin $(0, 0, 0)$. The unit vector in the direction of the solar plane is calculated as a combination of two cross products:

$$\mathbf{s}_p = \mathbf{s} \times \frac{\mathbf{s} \times \mathbf{s}_{xy0}}{|\mathbf{s} \times \mathbf{s}_{xy0}|}, \tag{20}$$

where the second term is the unit vector perpendicular to the Sun in the horizontal direction and $\mathbf{s}_{xy0}$ is (XY) plane. The projection $P'_{i,j}$ of $P_{i,j}$ is:

$$P'_{i,j} = \mathbf{P}_{i,j} \cdot \mathbf{s}_p \tag{21}$$

Figure 7. Hillshading of Mont Blanc DEM. The incident light is modified according to the cosine angle of incidence of the Sun on the slope. A minimum illuminance of 18% is introduced to account for diffuse radiation. Illumination is from the North-west at 45° elevation.

5. Sky view factor

The sky view factor is defined as the hemispherical fraction of unobstructed sky visible from any point (figure 8). This is an important parameter for the calculation of incoming diffuse radiation and for the net balance of long wave radiation (Dubayah

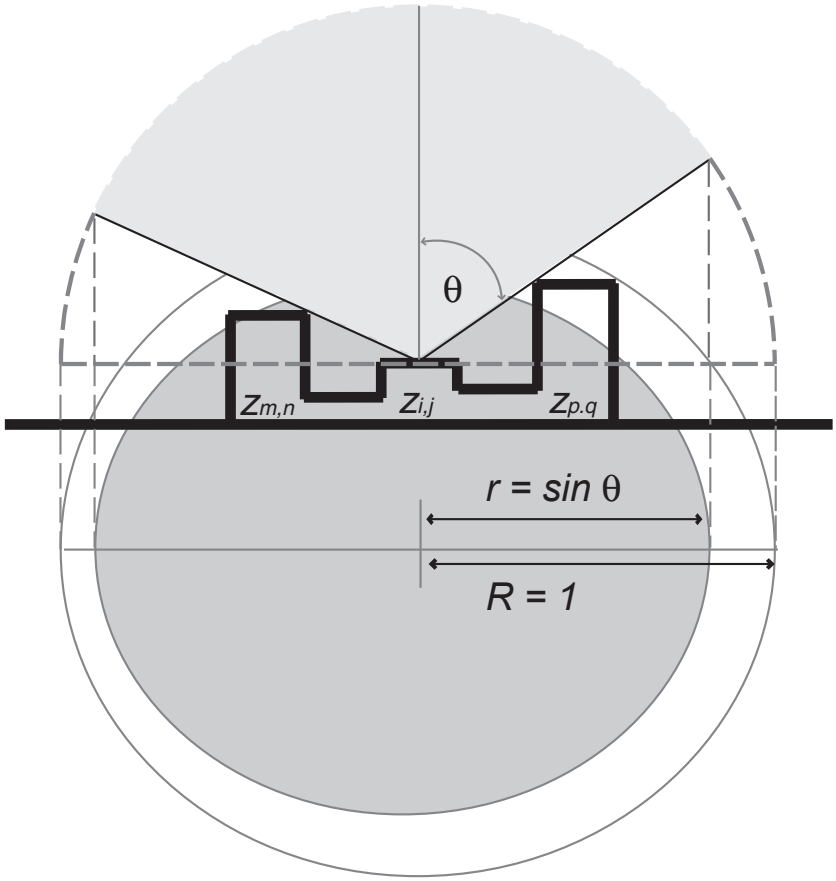

Figure 8. Sky view factor: the fraction of sky visible from any point is evaluated as the ratio of the projected area of the visible hemisphere to the area of the base of a unit sphere. The figure illustrates the calculation for a given cell $z_{i,j}$ with visibility obstructed by neighbouring cells $z_{m,n}$ and $z_{p,q}$, where the portion of visible sky is the shaded area. The sky view factor will be $r^2/R^2 = r^2 = \sin^2\bar{\theta}$, where $\bar{\theta}$ is the average zenithal angle for all azimuth directions. Note that for clarity in the illustration the projected visible surface area is selected only for two points and not for the average, thus the resulting geometry is an ellipse instead of a circle.

and Rich 1995, Duguay 1995, Varley *et al.* 1996). The complementary parameter, 'ground view factor', is important in the evaluation of diffuse and multiple scattered short wave radiation, especially in areas of high albedo, like snow covered mountains, as well as for the long wave radiative budget (Olyphant 1986a, 1986b, Greuell *et al.* 1997). It is also important in other fields, such as cosmogenic dating, in order to evaluate the topographical shielding from cosmic radiation (Dunne *et al.* 1999). It is a common practice to measure the zenithal angle of the horizon at a given azimuth interval and then average for all the compass directions to compute the ratio of visible hemisphere to the whole hemisphere (Nuñez 1980, Dozier and Frew 1990).

Following the unit-sphere method (Iqbal 1983, p. 298) the sky view factor is evaluated as the ratio of the projected surface of the visible part of the hemisphere, to the area of a whole hemisphere of unitary radius (figure 9). The radius of the projection of the visible part of the hemisphere is equal to the sine of the average

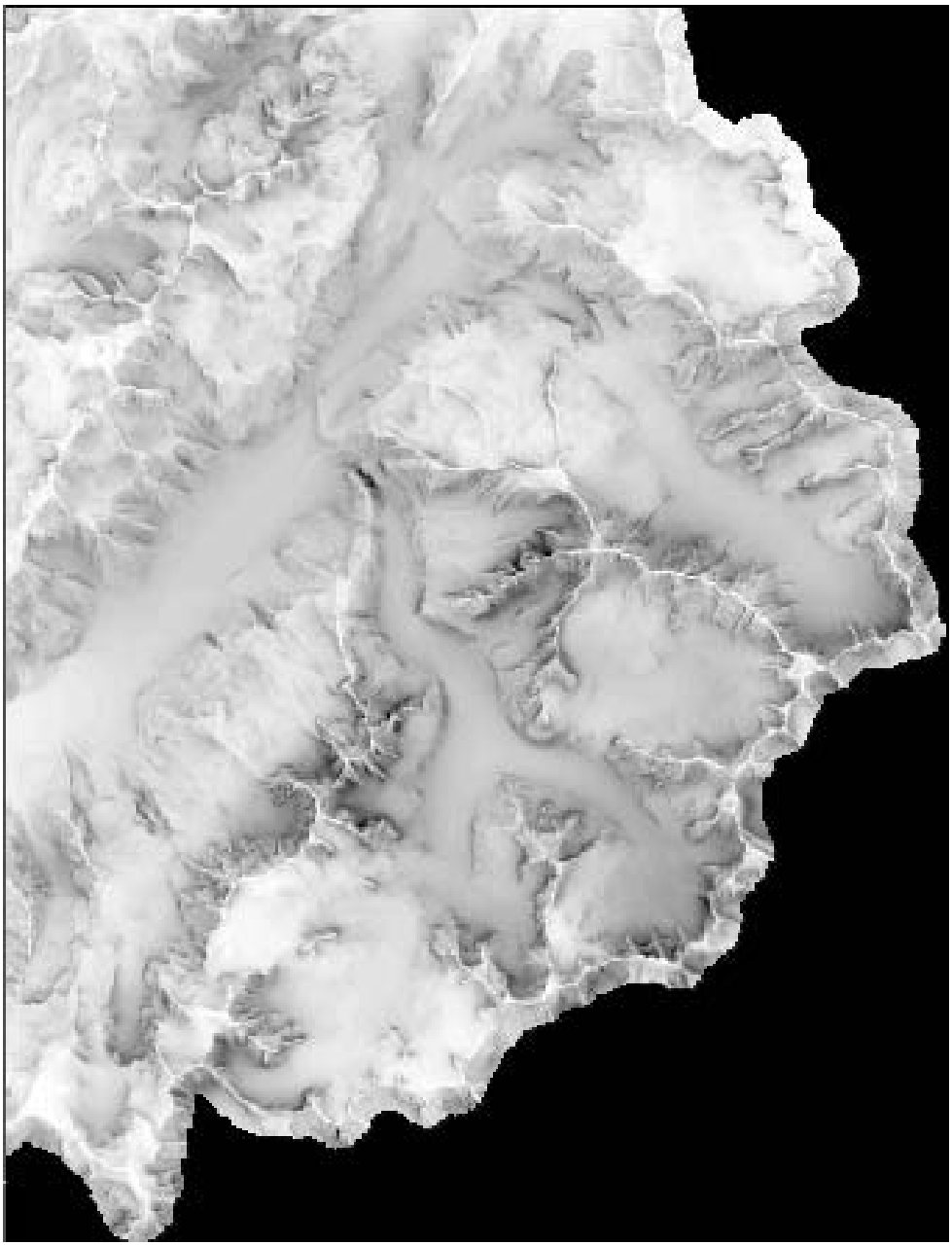

Figure 9. Relative grey-scale representation of sky view factor for the Mont Blanc DEM. Dark areas have lower sky visibility, while white ones, such as higher ridges, have unobstructed visibility of the upper hemisphere. Values range from 0.5 to 1, with the lowest value corresponding to the steepest slope, 81°, on the western face of Les Drus, centre right of the image.

zenithal angles in all azimuth directions. Here a variation of the hillshading algorithm described above is used to find the horizon zenithal angles for selected azimuths. By repeating the shading algorithm from a given azimuth direction in decreasing steps

of elevation values, we can find the horizon angles for every cell in that direction: this angle will be complementary to the current elevation angle at the cell's transition from Sun to shadow. The initial elevation value need not be higher than the maximum cell slope in the grid. This is repeated at the required azimuth interval over 360° and the results averaged. Thus the ratio of the two surfaces (visible and unobstructed hemispherical planar projections) will be:

$$v = \frac{\pi r^2}{\pi} = \sin^2 \bar{\theta}, \tag{22}$$

where v is the sky view factor, r is the radius of the circle corresponding to the planar projection of the visible sky and $\bar{\theta}$ is the average zenithal angle of the surrounding horizon.

A typical calculation for a terrain with slopes up to 45° and at 15° azimuthal intervals will require $45 \times 24 \times N$ operations if N is the number of cells in the DEM, which is considerably faster than the N^2 operations required for a rigorous estimation of all the angles subtended by every cell with any other cell in the grid.

Averaging $\bar{\theta}$ implies the assumption of isotropy in the diffuse radiation field, which is an unrealistic simplification. If this were not acceptable, the suggested algorithm can be used to store horizon angles at any given direction, at the expense of more memory requirements. For a rigorous evaluation of the influence of surrounding terrain on the radiation falling on any cell, it would be necessary to perform a viewshed analysis, rather than the simplified parameter 'ground view factor'. This point is not addressed here, but the reader is directed to the work of Wang *et al.* (2000a), which is probably the most efficient viewshed algorithm to date.

Dozier *et al.* (1981) have developed a very efficient algorithm for the calculation of local horizons that can be applied to the calculation of casted shadows. The shading algorithm in this paper might be more suitable for the calculation of shades at a limited number of illumination angles, as it is fast and does not need to store horizon information for every azimuth direction.

6. Comparison with other methods of calculating slope

It is questionable whether a synthetic surface is a valid comparison with real topography, but it has the advantage of providing error and artifact-free data. Similar approaches have been used successfully in the past (Hodgson 1995, 1998). Additionally, by choosing a continuous differentiable function to generate the surface, the gradient can be derived mathematically at every point, thus providing an analytical value for comparison.

A simple trigonometrical function with two terms, one for the base elevation and a second one to add a surface of rapidly changing relief, was chosen to generate a DEM of 10 000 cells sampled at regular intervals (figure 10). The function generating this surface is:

$$f(x, y, z) = -\cos x \cos y - a \sin bx \sin by + z = 0, \tag{23}$$

where a and b are constants with values 0.1 and 10 respectively.

The gradient of this function at any point x, y, z is calculated by finding the partial derivatives of every coordinate, as shown in appendix B. The results were compared to those obtained from the algorithms described here and with the output of a commonly used GIS software that uses a 3×3 kernel algorithm (ESRI 2000). The software manufacturer refers to Burrough (1986, p. 50, equation 3.4), which is

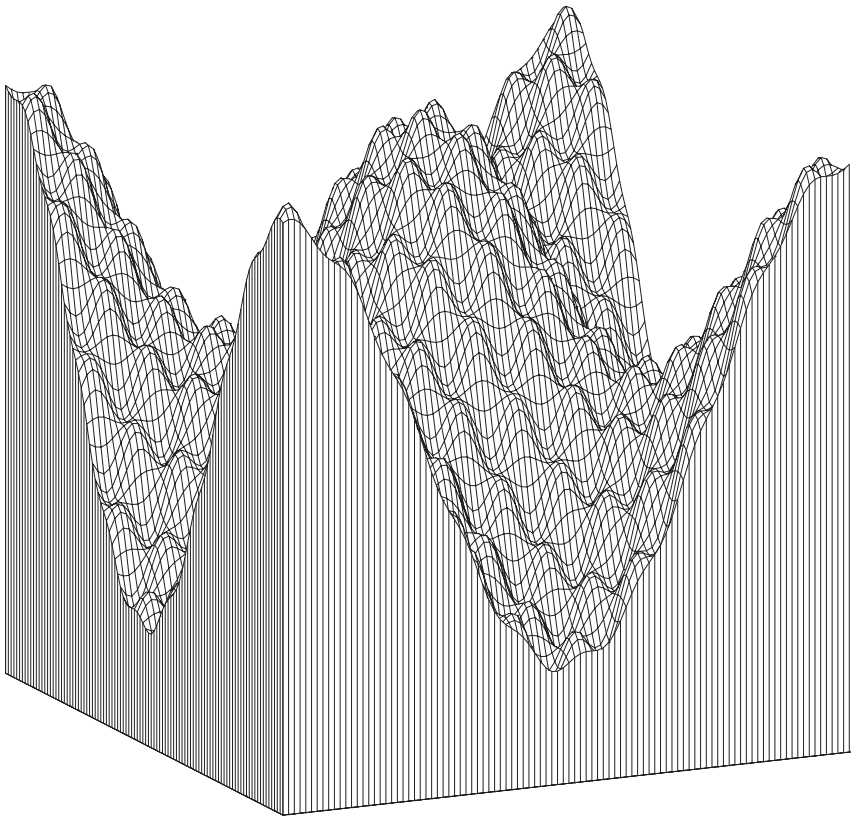

Figure 10. Synthetic DEM, a surface of highly variable relief generated by equation (23). Z values are in the range ± 1.07474, horizontal cell spacing is $2\pi/100$ units.

based on Horn (1981, p. 18). Figure 11 shows a scattergram comparing the slope values. Both algorithms underestimate the slope, although the vectorial algorithm is closer to the mathematically derived slope, presents less dispersion, smaller root mean square error, smaller standard deviation and less mean absolute deviation (table 1). Figure 12 shows a grey-scale representation of the spatial distribution of errors in the computation of slope for the synthetic DEM.

7. Conclusions

The algorithms described in this work are particularly suitable for surfaces of high and variable relief such as mountainous terrain. They minimize the area under evaluation, keeping extreme values with minimum smoothing. The new algorithm for the computation of the solar position permits straightfoward operation with the other terrain parameters, expressed as vectors. The main advantages of the algorithms described are the facility to operate vectors, the consistency of vector representation for all the procedures involved, easier conceptual visualisation in three dimensions and optimization of array handling capabilities in computer languages, which results in a fast and efficient implementation.

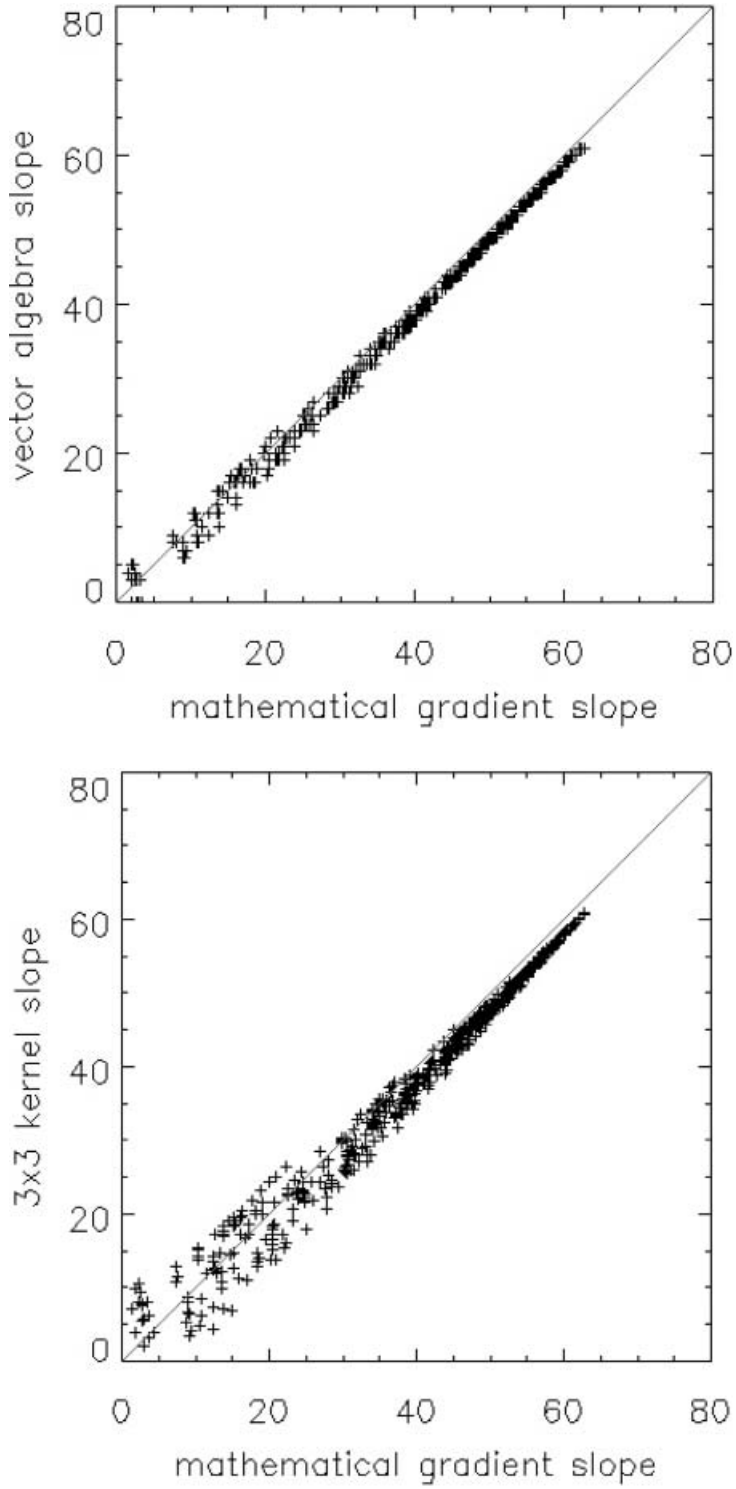

Figure 11. Scattergrams of slope values generated with the algorithm described in this paper and a 3×3 kernel algorithm compared to the slopes derived mathematically from a synthetic surface (figure 10 and equation (31)).

Table 1. Correlation between slopes derived mathematically from a synthetic surface and those calculated using the vector algebra algorithm and a 3×3 kernel algorithm.

Algorithm	Spearman's rank correlation	rms	σ	Mean absolute deviation
Math. gradient	—	—	—	—
Vector algebra	0.993804	0.7089	1.7993	0.8205
3×3 kernel	0.980826	1.2430	3.2623	1.7720

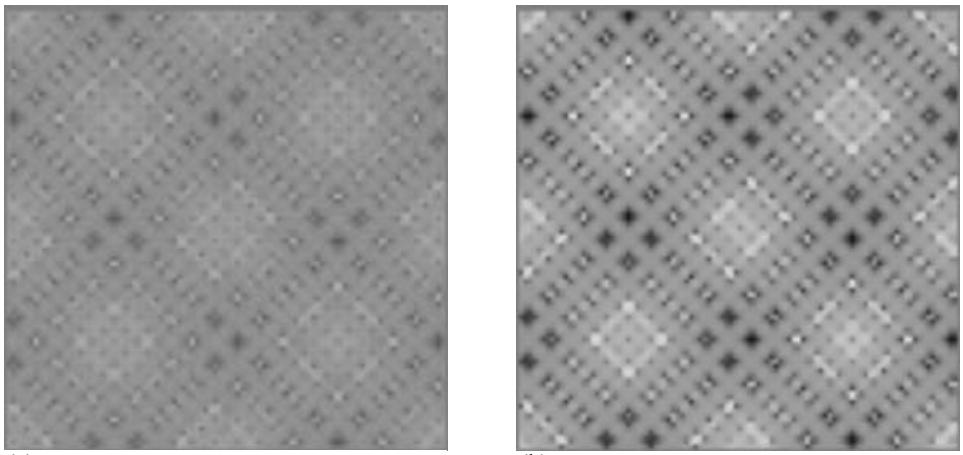

(a) (b)

Figure 12. Grey-scale representation of the spatial distribution of errors in the computation of slope for the synthetic DEM: (*a*) is between mathematically generated slopes and vector algorithm, (*b*) is the difference with the 3×3 kernel algorithm. Note that the location of errors is similar but these are accentuated in the right image. Values range from -2.91 to 3.78 and from -8.19 to 8.12. Neutral grey is no error, darker is overestimation and whiter is underestimation of slope.

Nomenclature

Symbol	Definition
$\mathbf{i}$	unit vector in the direction of the X-axis
$\mathbf{j}$	unit vector in the direction of the Y-axis
$\mathbf{k}$	unit vector in the direction of the Z-axis
l	grid cell length
$\mathbf{n}$	vector normal to the grid cell surface
$\mathbf{n}_u$	unit vector in the direction of $\mathbf{n}$
n_x	x-coordinate of vector $\mathbf{n}$
n_y	y-coordinate of vector $\mathbf{n}$
n_z	z-coordinate of vector $\mathbf{n}$
n_{xy}	projection of vector $\mathbf{n}$ on the XY-plane
$\mathbf{s}_0$	unit vector in the direction of the Sun at noon LAT
$\mathbf{s}$	unit vector in the direction of the Sun
δ	solar declination angle
γ	$=\pi/2-\varphi$, angle between topocentric Z-axis (along the Earth's radius at the observer position) and the axis of rotation of the Earth

ϕ	azimuth angle or aspect
φ	latitude
ς	slope gradient
θ	zenith angle
$\bar{\theta}$	average zenith angle of the horizon in all azimuth directions
θ_s	angle between Sun and normal to surface
v	sky view factor
ω	hour angle, zero at noon and positive before noon

Acknowledgments

I would like to express my gratitude to Ross Purves (University of Zürich) for lengthy discussions on these topics and for a detailed revision of the draft manuscript. This paper was written while enjoying a Carnegie Scholarship at the University of Edinburgh. I am also grateful to the anonymous reviewers for useful and referenced suggestions that improved the final content of this paper.

Appendix

A. Calculation of the solar vector coordinates

As γ is the angle between the Z-axis (or Earth's radius at the observer) and the Earth axis, it follows:

$$\gamma = \frac{\pi}{2} - \varphi, \tag{24}$$

thus, equation (9) can be expressed as:

$$\mathbf{s} = \begin{pmatrix} 1 & 0 & 0 \\ 0 & \sin\varphi & -\cos\varphi \\ 0 & \cos\varphi & \sin\varphi \end{pmatrix} \begin{pmatrix} \cos\omega & -\sin\omega & 0 \\ \sin\omega & \cos\omega & 0 \\ 0 & 0 & 1 \end{pmatrix} \begin{pmatrix} 1 & 0 & 0 \\ 0 & \sin\varphi & \cos\varphi \\ 0 & -\cos\varphi & \sin\varphi \end{pmatrix} \begin{pmatrix} s_{0x} \\ s_{0y} \\ s_{0z} \end{pmatrix} \tag{25}$$

Using the equivalences for the y and z coordinates of $\mathbf{s}_0$:

$$\mathbf{s}_{0y} = \sin(\varphi - \delta) = \sin\varphi\cos\delta - \cos\varphi\sin\delta \tag{26}$$

$$\mathbf{s}_{0z} = \cos(\varphi - \delta) = \cos\varphi\cos\delta - \sin\varphi\sin\delta \tag{27}$$

solving equation (25) and simplifying using $\sin^3 = \sin - \sin\cos^2$ and $\cos^3 = \cos - \cos\sin^2$, the x, y, z coordinates of the solar vector at hour angle ω will be:

$$\mathbf{s} = \begin{pmatrix} -\sin\omega\cos\delta \\ \sin\varphi\cos\omega\cos\delta - \cos\varphi\sin\delta \\ \cos\varphi\cos\omega\cos\delta + \sin\varphi\sin\delta \end{pmatrix}. \tag{28}$$

B. Gradient of synthetic surface

The gradient of function:

$$f(x,\ y,\ z) = -\cos x \cos y - a \sin bx \sin by + z = 0, \tag{29}$$

where a and b are constants is:

$$\nabla f(x, y, z) = \left(\frac{\partial f}{\partial x}\,\mathbf{i}, \frac{\partial f}{\partial y}\,\mathbf{j}, \frac{\partial f}{\partial z}\,\mathbf{k} \right) \tag{30}$$

Solving the partial derivatives gives the components of this vector

$$\nabla f(x, y, z) = \begin{Bmatrix} (\sin x \cos y - ab \cos bx \sin by)\,\mathbf{i} \\ (\cos x \sin y - ab \sin bx \cos by)\,\mathbf{j} \\ \mathbf{k} \end{Bmatrix}, \tag{31}$$

and from these, the slope, ς, is calculated as:

$$\varsigma = \cos^{-1} \frac{\nabla f_z}{|\nabla f|}. \tag{32}$$

References

Arnold, N. S., Willis, I. C., Sharp, M. J., Richards, K. S., and Lawson, M. J., 1996, A distributed surface energy-balance model for a small valley glacier. *Journal of Glaciology*, **42**, 77–89.

Barry, R. G., 1992, *Mountain Weather and Climate* (London: Routledge).

Bourges, B., 1985, Improvement in solar declination computation. *Solar Energy*, **35**, 367–369.

Brock, B. W., Willis, I. C., Sharp, M. J., and Arnold, N. S., 2000, Modelling seasonal and spatial variations in the surface energy balance of Haut Glacier d'Arolla, Switzerland. *Annals of Glaciology*, **31**, 53–62.

Burrough, P. A., 1986, *Principles of Geographical Information Systems for Land Resources Assessment* (New York: Oxford University Press).

Chang, K., and Tsai, B., 1991, The effect of DEM resolution on slope and aspect mapping. *Cartography and Geographic Information Systems*, **18**, 69–77.

Dakhal, A. M., Amada, T., and Aniya, M., 2000, Landslide hazard mapping and its evaluation using GIS: an investigation of sampling schemes for a grid-cell quantitative method. *Photogrammetric Engineering and Remote Sensing*, **66**, 981–989.

Dozier, J., Bruno, J., and Downey, P., 1981, A faster solution to the horizon problem. *Computers & Geosciences*, **7**, 145–151.

Dozier, J., and Frew, J., 1990, Rapid calculation of terrain parameters for radiation modelling from digital elevation data. *IEEE Transactions on Geoscience and Remote Sensing*, **28**, 963–969.

Dubayah, R., and Rich, P., 1995, Topographic solar radiation models for GIS. *International Journal of Geographical Information Systems*, **9**, 405–419.

Duguay, C. R., 1995, An approach to the estimation of surface net radiation in mountain areas using remote sensing and digital terrain data. *Theoretical and Applied Climatology*, **52**, 55–68.

Dunne, J., Elmore, D., and Muzikar, P., 1999, Scaling factors for the rates of production of cosmogenic nuclides for geometric shielding and attenuation at depth on sloped surfaces. *Geomorphology*, **27**, 3–11.

ESRI, 2000, Arc Info online documentation ArcDoc Version 8.0.2. Environmental Systems Research Institute technical documentation, Redlands, California.

Evans, I. S., 1980, An integrated system of terrain analysis and slope mapping. *Zeitschrift für Geomorphologie*, **Suppl-Bd 36**, 274–295.

Foley, J. D., van Dam, A., Feiner, S. K., and Hughes, J. F., 1990, *Computer graphics, principles and practice* (Reading, Massachusetts: Addison-Wesley).

Gao, J., 1997, Resolution and accuracy of terrain representation by grid DEMs at a micro-scale. *International Journal of Geographical Information Science*, **11**, 199–212.

Greuell, W., Knap, W. H., and Smeets, P. C., 1997, Elevational changes in meteorological variables along a midlatitude glacier during summer. *Journal of Geophysical Research*, **102**, 25 941–25 954.

Hodgson, M. E., 1995, What cell size does the computed slope/aspect angle represent? *Photogrammetric Engineering and Remote Sensing*, **65**, 513–517.

Hodgson, M. E., 1998, Comparison of angles from surface slope/aspect algorithms. *Cartography and Geographic Information Systems*, **25**, 173–185.

Horn, B. K. P., 1981, Hillshading and the reflectance map. *Proceedings of the IEEE*, **69**, 41–47.

Iqbal, M., 1983, *An Introduction to Solar Radiation* (Toronto: Academic Press).

Kirckpatrick, J. B., and Nuñez, M., 1980, Vegetation-radiation relationships in mountainous terrain: eucaliptus dominated vegetation in the Ridson Hill, Tasmania. *Journal of Biogeography*, **7**, 197–208.

Kumar, L., and Skidmore, A. K., 2000, Radiation-vegetation relationships in a eucalyptus forest. *Photogrammetric Engineering and Remote Sensing*, **66**, 193–204.

Kumar, L., Skidmore, A. K., and Nowles, E. K., 1997, Modelling topographic variation in solar radiation in a GIS environment. *International Journal of Geographical Information Science*, **11**, 475–497.

Moore, I. D., Gallant, J. C., Guerra, L., and Kalma, J. D., 1993, Modelling the spatial variability of hydrological processes using GIS. In *HydroGIS 93: Applications of Geographic Information Systems in Hydrology and Water Resources Management (Proceedings of the Vienna Conference, April 1993)* (Wallingford: IAMS), IAHS Publication no. 211, pp. 161–169.

Nautical Almanac Office, 1974, *Explanatory Supplement to the Astronomical Ephemeris and the American Ephemeris and Nautical Almanac* (London: HMSO).

Nuñez, M., 1980, The calculation of solar and net radiation in mountainous terrain (Risdon, Tasmania), *Journal of Biogeography*, **7**, 173–186.

Olyphant, G. A., 1986a, The components of incoming radiation within a mid-latitude Alpine watershed during the snowmelt season. *Arctic and Alpine Research*, **18**, 163–169.

Olyphant, G. A., 1986b, Longwave radiation in mountainous areas and its influence on the energy balance of alpine snowfields. *Water Resources Research*, **22**, 62–66.

Page, J. K. (editor), 1986, *Prediction of solar radiation on inclined surfaces*, Solar energy R & D in the European Community. Series F. Solar radiation data; v. 3, Dordrecht; Lancaster: Reidel for the Commission of the European Communities.

Peterson, W. A., Dirmhirn, I., and Hurst, R. L., 1985, A theoretical model to determine solar and diffuse irradiance in valleys. *Solar Energy*, **35**, 503–510.

Purves, R. S., Barton, J. S., Mackaness, W. A., and Sugden, D. E., 1998, The development of a rule-based spatial model of wind transport and deposition of snow. *Annals of Glaciology*, **26**, 197–202.

Richards, K., Sharp, M., Arnold, N., Gurnell, A., Clark, M., Tranter, M., Nienow, P., Brown, G., and Lawson, W., 1996, An integrated approach to modelling hydrology and water quality in glacierized catchments. *Hydrological Processes*, **10**, 479–508.

Ritter, P., 1987, A vector-based slope and aspect generation algorithm. *Photogrammetric Engineering and Remote Sensing*, **53**, 1109–1111.

Skidmore, A. K., 1989, A comparison of techniques for calculating gradient and aspect from a gridded digital elevation model. *International Journal of Geographical Information Systems*, **3**, 323–334.

Spencer, J. W., 1971, Fourier series representation of the position of the Sun. *Search*, **2**, 172.

Stefanovič, P., and Wiersema, G., 1985, Insolation from digital elevation models for mountain habitat evaluation. *ITC Journal*, **3**, 177–186.

Stocks, A. M., and Heywood, D. I., 1994, Terrain modelling for mountains. In *Mountain Environments and Geographic Information Systems*, edited by M. F. Price and D. I. Heywood (London: Taylor & Francis), pp. 25–40.

Varley, M. J., Beven, K. J., and Oliver, H. R., 1996, Modelling solar radiation in steeply sloping terrain. *International Journal of Climatology*, **16**, 93–104.

Wadge, G., 1988, The potential of GIS modelling of gravity flows and slope instabilities. *International Journal of Geographical Information Science*, **2**, 143–152.

WALRAVEN, R., 1977, Calculating the position of the Sun. *Solar Energy*, **20**, 393–397.

WANG, J., ROBINSON, G. J., and WHITE, K., 2000a, Generating viewsheds without using sightlines. *Photogrammetric Engineering and Remote Sensing*, **66**, 87–90.

WANG, J., WHITE, K., and ROBINSON, G., 2000b, Estimating surface net solar radiation by use of Landsat-5 TM and digital elevation models. *International Journal of Remote Sensing*, **21**, 31–43.

WILLIAMS, L. D., BARRY, R. G., and ANDREWS, J. T., 1972, Application of computed global radiation for areas of high relief. *Journal of Applied Meteorology*, **11**, 526–533.

WILLIS, I., ARNOLD, N., SHARP, M., BONVIN, J. M., and HUBBARD, B. P., 1998, Mass balance and flow variations in Haut Glacier d'Arolla, Switzerland, calculated using digital terrain modelling. In *Landform monitoring, modelling and analysis*, edited by S. Lane, K. Richards and J. Chandlers (Chichester: Wiley), pp. 343–362.

ZEVENBERGEN, L. W., and THORNE, C. R., 1987, Quantitative analysis of land surface topography. *Earth Surface Processes and Landforms*, **12**, 47–56.